Inorganic Chemistry
Article
Cite This: Inorg. Chem. XXXX, XXX, XXX−XXX
pubs.acs.org/IC

Remarkable Changes of the Acidity of Bound Nitroxyl (HNO) in the $[Ru(Me_3[9]aneN_3)(L^2)(NO)]^{n+}$ Family (n = 1−3). Systematic Structural and Chemical Exploration and Bioinorganic Chemistry Implications

Natalia Levin,[†] Nicolás Osa Codesido,[†] Juan Pablo Marcolongo,[†] Pablo Alborés,[†] Thomas Weyhermüller,[‡] José A. Olabe,[†] and Leonardo D. Slep*,[†]

[†]Departamento de Química Inorgánica, Analítica y Química Física, Facultad de Ciencias Exactas y Naturales, and INQUIMAE, Universidad de Buenos Aires, CONICET, Pabellón 2, 3er piso, Ciudad Universitaria, C1428EHA Ciudad Autónoma de Buenos Aires, Argentina

[‡]Max-Planck Institut für Chemische Energiekonversion, Stiftstraße 34−36, D-45470 Mülheim an der Ruhr, Germany

Supporting Information

ABSTRACT: This work demonstrates that the acidity of nitroxyl (HNO) coordinated to a metal core is significantly influenced by its coordination environment. The possibility that NO^- complexes may be the predominant species in physiological environments has implications in bioinorganic chemistry and biochemistry. This (apparently simple) result pushed us to delve into the basic aspects of HNO coordination chemistry. A series of three closely related $\{RuNO\}^{6,7}$ complexes have been prepared and structurally characterized, namely $[Ru(Me_3[9]aneN_3)(L^2)(NO)]^{3+/2+}$, with L^2 = 2,2′-bipyridine, 4,4′-dimethoxy-2,2′-bipyridine, and 2,2′-bipyrimidine. These species have also been thoroughly studied in solution, allowing for a systematic exploration of their electrochemical properties in a wide pH range, thus granting access and characterization of the elusive $\{RuNO\}^8$ systems. Modulation of the electronic density in the {RuNO} fragment introduced by changing the bidentate coligand L^2 produced only subtle structural modifications but affected dramatically other properties, most noticeably the redox potentials of the $\{RuNO\}^{6,7}$ couples and the acidity of bound HNO, which spans over a range of almost three pH units. Controlling the acidity of coordinated HNO by the rational design of coordination compounds is of fundamental relevancy in the field of inorganic chemistry and also fuels the growing interest of the community in understanding the role that different HNO-derived species can play in biological systems.

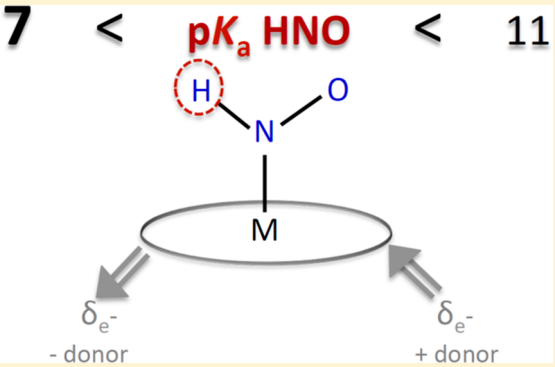

INTRODUCTION

Several metabolic and signaling processes rely on the interaction between metalloproteins and small molecules, which may bind to their metal centers. The number of relevant species is constantly growing and includes, among others, nitric oxide (NO), carbon monoxide (CO), and hydrogen sulfide (SH_2).[1] NO already has a well-gained reputation as a signaling molecule under physiological conditions in vascular processes and as the first gas neurotransmitter ever discovered.[2] Its main signaling pathway is currently considered to involve coordination to the iron(II)-heme site of metalloprotein sGC, the universal sensor and receptor of NO in mammals.[3] Activation of the enzyme would be triggered by NO binding, thus inducing labilization of a hystidine ligand located in the trans position to NO. This trans effect has also been observed in several hexacoordinated $\{MNO\}^7$ species (M = Fe, Ru).[4] The redox chemistry associated with the diatomic NO molecule is fascinating. It involves conversion to nitrosonium (NO^+, the one-electron oxidation product) and nitroxyl (NO^-, the one-electron reduction product). While free NO^+ is extremely reactive in water, forming nitrite at biorelevant pH values, it displays a rich coordination chemistry and reactivity, mainly due to the attack of diverse types of nucleophiles (OH^-, amines, thiolates, etc.).[5] Much less understood is the chemistry of free and coordinated nitroxyl, NO^-,[5] which also displays a complex acid−base reactivity involving the formation of HNO.[6] There are indications that the latter species could also function as a signaling agent in biochemical processes, but with functions different (though partially overlapping) from those of NO.[7] Both molecules can target the cardiovascular system, can be involved in redox processes, and could act as potential therapeutic agents,[8] with HNO being a promising novel pharmacological agent for different conditions (heart failure, ischemia reperfusion, alcoholism, etc.).[7b] Even when NO and NO^-/HNO could bind sGC in a similar way, it has been proposed that only NO and NO^- would be able to activate the

Received: July 13, 2018

Downloaded via UNIV DE BUENOS AIRES on September 18, 2018 at 12:22:23 (UTC).
See https://pubs.acs.org/sharingguidelines for options on how to legitimately share published articles.

© XXXX American Chemical Society

DOI: 10.1021/acs.inorgchem.8b01958
Inorg. Chem. XXXX, XXX, XXX−XXX

enzyme because of their strong trans effect,[4a,b] in contrast to the negligible influence of HNO. The latter is an elusive molecule, and its biological chemistry is under rigorous scrutiny.[9] It is believed to be generated primarily in body fluids by the oxidation of L-arginine promoted by iron(II)-based NO-synthase enzymes in a mechanism not yet fully understood.[3b,9] Its chemistry is currently investigated by employing the so-called "HNO donors", like the dianion of Angelis' salt, trioxidonitrate $N_2O_3^{2-}$.[10] Once released into aqueous solution, the HNO molecule has a short lifetime, which is just long enough to perform reactivity studies on highly biorelevant substrates such as dioxide (O_2), thiols, and transition-metal centers.[11] These reactions, though, always compete with the fast generation of nitrous oxide (N_2O) in a pH-dependent HNO-dimerization process that involves hyponitrite intermediates.[11,12] Because of its facile oxidation, it has been suggested that the alleged biological effects of HNO might actually be due to a previous conversion to NO.[13] Part of the controversy around this and other related issues has to do with the fact that basic aspects of the redox and acid−base properties of coordinated HNO are still far from clearly understood. Free HNO has been studied in gas-phase and water solutions for many years, both experimentally and theoretically.[6] Its acidity constant has been the focus of several reports since the 1970s. Upon revision of the earlier proposed value of 4.7,[6a] the pK_a values for the conversion of HNO into $^3NO^-$ and $^1NO^-$ have been established as 11.4 and 23, respectively.[6b] On the contrary, there are only a few HNO-carrying nonheme and heme coordination compounds well suited for studies in water.[5,14] As a consequence, questions apparently as trivial as the protonation status of coordinated HNO under physiological conditions are not well understood. Because the ground state of coordinated NO^- has been associated with the closed-shell singlet configuration,[15] it has been assumed that, even after coordination, HNO should remain protonated at pH close to neutral, despite the Lewis acidity influence of the metal center. This is a nontrivial assumption because, as we mentioned above, HNO and NO^- display completely different σ-donor capabilities and therefore different trans effect power.[4a,b] Being able to unambiguously assess whether HNO or NO^- is present at a certain physiological pH becomes a key piece of information to unravel the biological functions that these molecules may have.

Our group reported the first complete spectroscopic, redox, and acid−base characterization of a ruthenium-based nitrosyl system in water,[16] covering three different redox states, $\{RuNO\}^{6,7,8}$.[17] This report, which also explored the structure of the isolated perchlorate salt of the 3+ cation, ($[Ru(Me_3[9]aneN_3)(bpy)(NO)][ClO_4]_3$), ($Me_3[9]aneN_3$ = 1,4,7-trimethyl-1,4,7-triazacyclononane; bpy = 2,2′-bipyridine), was complemented later by the preparation of $[Ru(Me_3[9]aneN_3)(bpy)(NO)](BF_4)_2$ ($[\mathbf{1\text{-}NO}](BF_4)_2$), the first structurally characterized $\{RuNO\}^7$ species.[18] The experimental pK_a value for HNO in $[Ru(Me_3[9]aneN_3)(bpy)(HNO)]^{2+}$ ($[\mathbf{1\text{-}HNO}]^{2+}$) turned out to be close to 10, noticeably smaller than that observed for free HNO, suggesting that the impact of coordination might be more important than expected. One might argue that this enhancement of the acidity of HNO would not affect its protonation status under physiological conditions, but in the absence of reliable pK_a determinations, it is problematic to extrapolate this conclusion to other coordination compounds of HNO.

The $\{Ru(Me_3[9]aneN_3)(bpy)\}$ core employed in the mentioned reports proved to be robust and easy to handle in solution. We therefore envisioned the possibility of exploring slight modifications of the coligand environment by replacing the bpy ligand by similar ones with different donor/acceptor capabilities. We report here the preparation and full characterization for such species and show that, in spite of the subtle structural changes induced by the replacement of the bidentate coligand, the impact on the redox potentials of the $\{RuNO\}^{6,7}$ couples, and particularly on the pK_a of bound HNO, is remarkable.

■ EXPERIMENTAL SECTION

Materials and Reagents. The reagents employed in the synthetic procedures were purchased from Sigma-Aldrich and used without further purification. All organic solvents employed in synthetic procedures or physical determinations were dried and freshly distilled before use following standard procedures.[19] Vacuum-line and Schlenk glassware (or alternatively a glovebox) was employed when the manipulation required the exclusion of air. $[Ru(Me_3[9]aneN_3)(bpy)(H_2O)](BF_4)_2$ ($[\mathbf{1\text{-}H_2O}](BF_4)_2$) and $[Ru(Me_3[9]aneN_3)(MeObpy)(H_2O)](BF_4)_2$ ($[\mathbf{2\text{-}H_2O}](BF_4)_2$) were prepared according to published procedures,[20] replacing the precipitating agent $NaClO_4$ by $NaBF_4$. $[Ru(Me_3[9]aneN_3)(bpy)(NO)](BF_4)_2$ ($[\mathbf{1\text{-}NO}](BF_4)_2$) was prepared according to ref 18.

Synthesis of the Compounds. *$[Ru(Me_3[9]aneN_3)(bpy)(NO_2)](BF_4)$ ($[\mathbf{1\text{-}NO_2}](BF_4)$).* This species was prepared following the procedure[21] reported for $[\mathbf{1\text{-}NO_2}](ClO_4)$ but employing $[\mathbf{1\text{-}H_2O}](BF_4)_2$ as a precursor and replacing the precipitating agent $NaClO_4$ by $NaBF_4$. Yield: 176 mg (78%). Anal. Calcd for $[\mathbf{1\text{-}NO_2}](BF_4)$, $C_{19}H_{29}N_6O_2BF_4Ru$ (MW = 561.35 g·mol^{-1}): C, 40.7; H, 5.2; N, 15.0. Found: C, 39.6; H, 4.6; N, 13.8. MS (ESI$^+$): m/z 475.1 ($[M - BF_4^-]^+$).

$[Ru(Me_3[9]aneN_3)(MeObpy)(NO_2)](BF_4)$ ($[\mathbf{2\text{-}NO_2}](BF_4)$). A mixture of $Ru(Me_3[9]aneN_3)Cl_3$ (226 mg, 0.597 mmol), 4,4′-dimethoxy-2,2′-bipyridine (MeObpy; 144 mg, 0.666 mmol), and Zn metal powder (696 mg) was suspended in 70 mL of water and refluxed under an Ar atmosphere. After 1 h, the excess of Zn was removed by filtration, yielding a burgundy solution of the aquo complex $[\mathbf{2\text{-}H_2O}]^{2+}$. Further reflux of the latter after the addition of sodium nitrite (865 mg, 12.54 mmol) afforded a bright-red solution after 1 h of reaction. The reaction mixture was treated with 1 mL of 0.1 M NaOH, and the solution was reduced to 5 mL by means of a rotatory evaporator. Solid NH_4BF_4 (632 mg, 6.02 mmol) was added, and the solution was left overnight at 4 °C. Bright-red crystals were collected by filtration, washed with cold water, and vacuum-dried. Yield: 242 mg (65%). Anal. Calcd for $[\mathbf{2\text{-}NO_2}](BF_4)$, $C_{21}H_{33}N_6O_4BF_4Ru$ (MW = 621.41 g·mol^{-1}): C, 40.6; H, 5.4; N, 13.5. Found: C, 40.1; H, 4.8; N, 13.0. MS (ESI$^+$): m/z 535.2 ($[M - BF_4^-]^+$). The product was alternatively obtained by reflux of $[\mathbf{2\text{-}H_2O}](BF_4)_2$ (prepared following the published procedure[20b] for $[\mathbf{2\text{-}H_2O}](ClO_4)_2$ but replacing the precipitating agent $NaClO_4$ for $NaBF_4$) with sodium nitrite.

$[Ru(Me_3[9]aneN_3)(MeObpy)(NO)](BF_4)_2$ ($[\mathbf{2\text{-}NO}](BF_4)_2$). A total of 75 mg (0.121 mmol) of $[\mathbf{2\text{-}NO_2}](BF_4)$ was dissolved in 10 mL of acetone to afford a red solution. The addition of 1 drop of trifluoromethanesulfonic acid turned the solution yellow, a property of the nitrosonium species $[2\text{-}NO]^{3+}$. Throughout the procedure the reaction medium was protected from light and kept under Ar. After 8 mL of a deaerated saturated solution of KI in acetone was added dropwise, the solution turned brown, and as the addition continued, a brown-gray precipitate developed. Solid $[\mathbf{2\text{-}NO}]I_2$ was collected by filtration. The IR spectrum of the precipitate showed a band at 1620 cm^{-1}, characteristic of a $\{RuNO\}^7$ compound. The precipitate was dissolved in 14 mL of deaerated distilled water containing 28 mg of NH_4BF_4. Overnight slow evaporation with an Ar flow afforded dark crystals suitable for XRD analysis. The resulting crystals revealed a small but quantifiable amount of iodide as a counterion. Analysis of the XRD data afforded $[\mathbf{2\text{-}NO}](BF_4)_{1.97}I_{0.03}$ as the most probable

DOI: 10.1021/acs.inorgchem.8b01958
Inorg. Chem. XXXX, XXX, XXX−XXX

stoichiometry for the single crystal. The compound isolated in this manner was only used for structural characterization. The same procedure employed for the synthesis of [**1-NO**]$(BF_4)_2$ was also repeated with the starting reagent [**2-NO$_2$**](BF_4) and afforded a pure dark powder, although unsuitable for XRD analysis. Anal. Calcd for [**2-NO**]$(BF_4)_2$, $C_{21}H_{33}N_6O_3B_2F_8Ru$ (MW = 692.21 g·mol^{-1}): C, 36.4; H, 4.8; N, 12.1. Found: C, 35.2; H, 4.4; N, 11.4. MS (ESI$^+$): *m/z* 606.2 ([M − BF_4^-]$^+$), 259.6 ([M − 2BF_4^-]$^{2+}$). ν_{NO} = 1606 cm^{-1} (ATR).

*[Ru(Me$_3$[9]aneN$_3$)(bpym)(NO)](BF$_4$)$_3$ ([**3-NO**](BF$_4$)$_3$).* Ru(Me$_3$[9]-aneN$_3$)Cl$_3$ (200 mg, 0.529 mmol), 2,2′-bipyrimidine (bpym; 256 mg, 1.62 mmol) and Zn metal powder (570 mg) suspended in 40 mL of deaerated water were refluxed in an Ar atmosphere for 1 h, upon which the solution turned burgundy. After filtration of excess Zn, the solution of [**3-H$_2$O**]$^{2+}$ was refluxed again in an Ar atmosphere with sodium nitrite (732 mg, 10.6 mmol) to afford an orange solution after 1 h of reaction. Upon the addition of 4 mL of HBF_4, the volume of the solution was reduced by a rotatory evaporator and left for 2 weeks at 4 °C. Yellow crystals of [**3-NO**]$(BF_4)_3$·2H_2O suitable for XRD analysis were collected. Yield: 239 mg (63%). Anal. Calcd for [**3-NO**]$(BF_4)_3$, $C_{17}H_{27}N_8O_1B_3F_{12}Ru$ (MW = 720.93 g·mol^{-1}): C, 28.3; H, 3.8; N, 15.5. Found: C, 27.2; H, 4.0; N, 14.8. MS (ESI$^+$): *m/z* 635.1 ([M − BF_4^-]$^+$), 153.7 ([M − 3BF_4^-]$^{3+}$). ν_{NO} = 1947 cm^{-1} (ATR).

*[Ru(Me$_3$[9]aneN$_3$)(bpym)(NO)](BF$_4$)$_2$ ([**3-NO**](BF$_4$)$_2$).* The same procedure as that employed in the synthesis of [**1-NO**]$(BF_4)_2$ was used,[18] replacing the starting reagent [**1-NO$_2$**](BF_4) by [**3-NO**]-$(BF_4)_3$, affording also crystals of [**3-NO**]$(BF_4)_2$ suitable for X-ray analysis. Anal. Calcd for [**3-NO**]$(BF_4)_2$, $C_{17}H_{27}N_8O_1B_2F_8Ru$ (MW = 634.13 g·mol^{-1}): C, 32.2; H, 4.3; N, 17.7. Found: C, 30.1; H, 4.4; N, 16.1. MS (ESI$^+$): *m/z* 548.1 ([M − BF_4^-]$^+$), 230.3 ([M − 2BF_4^-]$^{2+}$). ν_{NO} = 1606 cm^{-1} (ATR).

Physical Measurements. UV−vis spectra were recorded with either an HP8453 or an HP8452A diode-array spectrometer. IR spectral measurements were carried out in KBr pellets, using a Thermo Nicolet AVATAR 320 or in ATR mode using a Thermo Nicolet iS50 FT IR spectrometer. Microanalytical data for C, H, and N were obtained with a Carlo Erba EA 1108 analyzer. Electrospray ionization (ESI) mass spectrometry (MS) spectra were obtained with a standard ESI source and Q Exactive Plus from ThermoFisher Scientific equipment. X-band electron paramagnetic resonance (EPR) spectra were recorded at 85 K with a Bruker ESP 300 spectrometer equipped with an Oxford ESR 910 liquid-helium cryostat and an Oxford temperature controller. X-band EPR spectra were simulated with *EasySpin 5.0.9*.[22] ^{1}H NMR spectra were measured with a 500 MHz Bruker AM 500 spectrometer; chemical shifts are referred to tetramethylsilane.

Cyclic voltammetry (CV) and square-wave voltammetry (SWV) measurements in acetonitrile employing 0.1 M Bu_4NPF_6 as the supporting electrolyte were performed with a standard three-electrode cell containing a working vitreous C electrode (3 mm Φ), a Pt wire as the counter electrode, and a Ag wire plus an internal ferrocene (Fc) standard as the reference electrode. In water, we employed a similar arrangement except that the reference was a standard Ag/AgCl (3 M NaCl) commercial electrode (BAS). The potential of the working electrode was controlled with a TEQ-03 or a Bio-Logic SP-300 potentiostat. The spectroelectrochemical experiments in the UV−vis region were done in a homemade cell containing a quartz cuvette (1 cm path length). In all cases, the ionic strength *I* was fixed to 1 M with NaCl in water or 0.1 M Bu_4NPF_6 in acetonitrile. The Ag/AgCl (3 M NaCl) and Ag/$AgNO_3$ (0.01 M) electrodes were used as references in an aqueous solution and an organic medium, respectively. The working electrode was a Pt net, and the counter electrode was a Pt wire. The system was maintained at 25.0 ± 0.1 °C for the experiments in water and at −30 ± 1 °C for those in acetonitrile (RC6 LAUDA thermostat) and entirely purged with Ar. Throughout this work, all of the reported redox potentials are referred to Ag/AgCl and 3 M NaCl (0.21 V vs NHE). A typical spectroelectrochemical experiment required the application for a short period of time of a cathodic potential that induced charge circulation at the working electrode. Then electrolysis was interrupted to allow homogenization of the solution and simultaneous recording of the electronic spectrum and open-circuit potential of the solution. The redox potentials and disclosed UV−vis spectra of all of the species present in solution were obtained by global analysis.[23] The procedure involved a simultaneous multiwavelength fitting, assuming that all of the redox-active couples present in solution behave according to the Nernst equation.[16,24] pH-dependent experiments in water required different buffer solutions, depending on the pH. Kinetic studies for the addition of OH^- to yield the corresponding nitro species were done under pseudo-first-order conditions, at *I* = 1 M (NaCl). Solutions at different [OH^-] were prepared by mixing 1 mL of a 6.31 × 10^{-5} M solution of [**1-NO**]$^{3+}$, [**2-NO**]$^{3+}$, or [**3-NO**]$^{3+}$ (0.01 M HCl, *I* = 1 M NaCl) with 1 mL of the appropriate ($H_2PO_4^-$/HPO_4^{2-} or a H_3BO_3/$B(OH)_4^-$) buffer solution (0.33 M, *I* = 1 M NaCl) in a 1 cm path length quartz cuvette. In all cases, the pH was checked after each kinetic run. The pseudo-first-order kinetic constants k_{obs} were obtained by multiwavelength global analysis employing data measured in the UV−vis−near-IR range. Plots of k_{obs} versus [OH^-] were employed to calculate the second-order rate constant (see the text). Rate constants, k_{OH}, at different temperatures (range of 20−40 °C) were employed to estimate the activation parameters (enthalpies and entropies) through an Eyring plot, ln(k_{OH}/T) versus $1/T$. Determination of the equilibrium constant for the addition of OH^- was performed spectrophotometrically by employing equilibrated solutions containing [**1-NO**]$^{3+}$, [**2-NO**]$^{3+}$, or [**3-NO**]$^{3+}$ at different pH values ($H_2PO_4^-$/HPO_4^{2-}, 0.33 M buffer solution, *I* = 1 M NaCl). The solutions were allowed to equilibrate for 24 h before the spectra were recorded and then treated by employing global analysis techniques described elsewhere.[16,21,24b,c,25]

X-ray Crystallographic Data Collection and Refinement of the Structures. The crystal structures of compounds [**1-NO**]$(BF_4)_3$, [**2-NO**]$(ClO_4)_3$·H_2O, [**3-NO**]$(BF_4)_3$·2H_2O, [**1-NO**]$(BF_4)_2$ were determined with an Oxford Xcalibur, Eos, Gemini CCD area-detector diffractometer using graphite-monochromated Mo Kα radiation (λ = 0.71069 Å) at 293 K in the cases of [**2-NO**]$(ClO_4)_3$·H_2O and [**3-NO**]$(BF_4)_3$·2H_2O and at 170 K for complexes [**1-NO**]$(BF_4)_2$ and [**1-NO**]$(BF_4)_3$. Data were corrected for absorption with *CrysAlisPro*, version 1.171.33.66, Oxford Diffraction Ltd., by applying an empirical absorption correction using spherical harmonics, as implemented in the *SCALE3 ABSPACK* scaling algorithm.[26] The structures were solved by direct methods with *SIR97*[27] and refined by full-matrix least squares on F^2 with *SHELXL-2014*[28] under the *WinGX* platform.[29] H atoms were added geometrically and refined as riding atoms with a uniform value of U_{iso}. In the complex [**3-NO**]$(BF_4)_3$·2H_2O structure, one tetrafluoroborate anion was found to be disordered around two positions and anisotropically refined with 0.5:0.5 fixed occupancy factors. Solvent water H^+ ions were not located in the difference map; hence, they were geometrically fixed following short-contact most feasible interactions. In the case of complex [**2-NO**]$(ClO_4)_3$·H_2O structure, two of the three perchlorate anions appeared disordered around two positions and were anisotropically refined with 0.5:0.5 fixed occupancy factors. Water solvent H atoms were located in the difference map and refined as riding atoms over the O atom with a uniform U_{iso} value. The final crystallographic data and values of R_1 and wR_2 are listed in Table A. CCDC 1463223, 1852505, 1852506, and 1852507 contain the supplementary crystallographic data for [**1-NO**]$(BF_4)_2$, [**1-NO**]$(BF_4)_3$, [**2-NO**]$(ClO_4)_3$·H_2O, and [**3-NO**]-$(BF_4)_3$·2H_2O, respectively.

The crystal structures of compounds [**2-NO**]$(BF_4)_{1.97}I_{0.03}$ and [**3-NO**]$(BF_4)_2$ were determined using a Bruker-Nonius Kappa Mach3/APEX II diffractometer equipped with a Mo IμS anode and INCOATEC Helios mirror optics (λ = 0.71073 Å). Diffraction data were collected at 100 K in a N_2 cryostream. The final cell constants were obtained from least-squares fits of several thousand strong reflections. The intensities of redundant reflections were used to correct for absorption using the program *SADABS*.[30] The structure was readily solved by Patterson methods and subsequent difference Fourier techniques. The Siemens *ShelXTL* software package[31] was used for solution and artwork of the structures, and *ShelXL-2013*[32]

DOI: 10.1021/acs.inorgchem.8b01958
Inorg. Chem. XXXX, XXX, XXX−XXX

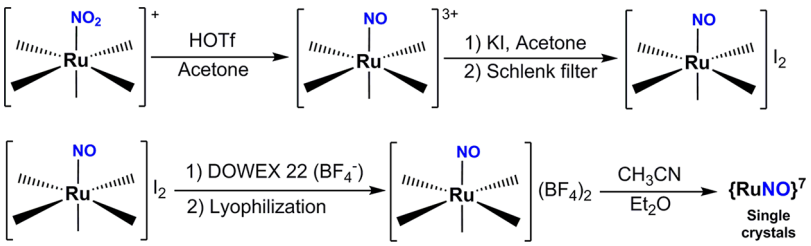

Figure 1. Synthetic strategy employed in the preparation and isolation of the $\{RuNO\}^7$ species.

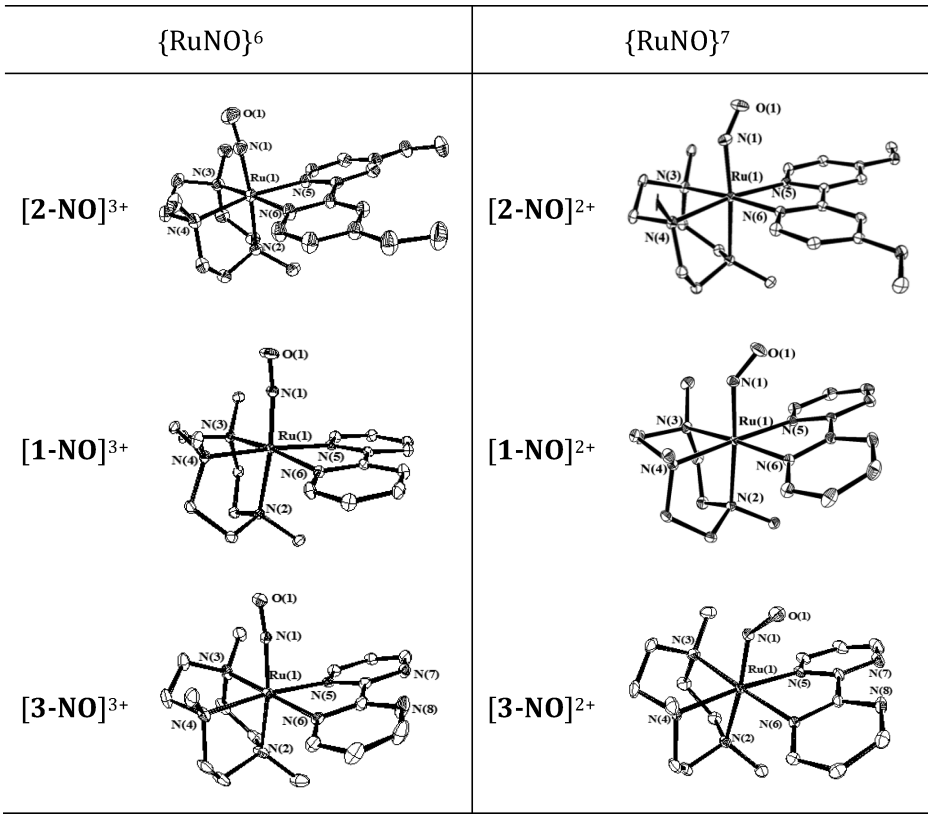

Figure 2. Structures of the cations (30% probability level thermal ellipsoids) in the crystals of [**2-NO**]$(ClO_4)_3 \cdot H_2O$, [**1-NO**]$(BF_4)_3$, and [**3-NO**]$(BF_4)_3 \cdot 2H_2O$ (left column) and [**2-NO**]$(BF_4)_2$, [**1-NO**]$(BF_4)_2$, and [**3-NO**]$(BF_4)_2$(right column).

was used for structure refinement. All non-H atoms were anisotropically refinedm and H atoms bound to C were placed at calculated positions and refined as riding atoms with isotropic displacement parameters. A split atom model with restrained atomic displacement parameters and bond lengths was refined using the *ShelXL* EADP, SADI, and ISOR instructions. The occupation factor ratios refined to values of about 0.6:0.4 and 0.67:0.33, respectively. CCDC 1852828 and 1852829 contain the supplementary crystallographic data for [**2-NO**]$(BF_4)_{1.97}I_{0.03}$ and [**3-NO**]$(BF_4)_2$, respectively.

Theoretical Calculations. We employed density functional theory (DFT) computations to fully optimize the ground-state geometries of all of the species described in this work. The calculations were done with *Gaussian 09*[33] using Becke's three-parameter hybrid functional, with the correlation functional of Lee, Yang, and Parr formalized as the B3LYP hybrid functional[34] and the effective core potential basis set LanL2DZ,[35] which proved to be suitable for geometry predictions in coordination compounds containing metals of the second row of transition elements in the Periodic Table. We used tight self-consistent-field convergence criteria and default settings in the geometry optimizations. For the species holding bent Ru−N−O moieties, the computations involved a potential energy surface scan of the dihedral O−N−Ru−N(bpy) angle, which revealed in all cases two possible local minima corresponding roughly to a 180° change in the above-mentioned dihedral angle. The nature of the resulting stationary points was in all cases tested by computing the vibrational spectrum. The geometry of the two conformers obtained for each species turned out to be very similar, with practically identical coligand environments except for the disposition of the NO fragment. The explored potential energy surfaces were rather flat with small energy barriers between conformers compatible with free rotation of the NO moiety.

Analysis of the electronic structure was complemented with time-dependent DFT (TDDFT) computations including up to 70 states of the same multiplicity as the ground state. The spectra were computed at the gas-phase geometry of the lowest-energy conformer of each species, and solvation effects in aqueous solution were taken into account by employing the polarizable continuum model (PCM) approximation, as implemented in *Gaussian 09*.

RESULTS AND DISCUSSION

Synthesis and Structural Characterization. The reaction of $Ru(Me_3[9]aneN_3)Cl_3$ with the bidentate ligands L^2 = bpy, MeObpy, or bpym in aqueous solution in the presence of metallic Zn provides an effective way to prepare the aquo complexes $[Ru(Me_3[9]aneN_3)(L^2)(H_2O)]^{2+}$.[20] These species

DOI: 10.1021/acs.inorgchem.8b01958
Inorg. Chem. XXXX, XXX, XXX−XXX

Table 1. Crystallographic Data of the Isolated {RuNO}^{6,7} Species

	[**2-NO**]$(ClO_4)_3\cdot H_2O$	[**1-NO**]$(BF_4)_3$	[**3-NO**]$(BF_4)_3\cdot 2H_2O$	[**2-NO**]$(BF_4)_{1.97}I_{0.03}$	[**1-NO**]$(BF_4)_2$	[**3-NO**]$(BF_4)_2$
formula	$C_{21}H_{33}N_6O_{16}Cl_3Ru$	$C_{19}H_{29}B_3F_{12}N_6ORu$	$C_{17}H_{31}B_3F_{12}N_8O_3Ru$	$C_{21}H_{33}(BF_4)_{1.97}I_{0.03}N_6O_3Ru$	$C_{19}H_{29}B_2F_8N_6ORu$	$C_{17}H_{27}B_2F_8N_8O_1Ru$
M_r	834.97	718.98	757.00	692.21	632.16	634.13
cryst syst	orthorhombic	orthorhombic	monoclinic	monoclinic	monoclinic	triclinic
space group	*Pbca*	*Pbca*	*P*21/*c*	*P*21/*n*	*P*21/*n*	$P\bar{1}$
a/Å	18.0483(7)	14.9695(3)	9.8749(3)	8.3161(6)	11.068(5)	11.274(2)
b/Å	18.6446(7)	11.5909(2)	28.2891(10)	8.5161(5)	10.714(5)	14.9603(7)
c/Å	19.0596(9)	30.6857(6)	10.0503(4)	37.375(2)	20.824(5)	15.080(2)
V/Å^3	6413.6(6)	5324.28(18)	2786.99(17)	2445.0(3)	2436.0(17)	2440.3(6)
α/deg	90	90	90	90	90	86.571(6)
β/deg	90	90	96.942(5)	92.164(5)	99.431(5)	73.993(10)
γ/deg	90	90	90	90	90	89.592(7)
Z	8	8	4	4	4	4
D_{calc}/Mg·m^{-3}	1.729	1.794	1.804	1.741	1.724	1.726
T/K	293(2)	170(2)	293(2)	100(2)	170(2)	100(2)
μ/mm^{-1}	0.820	0.701	0.681	0.721	0.731	0.732
data/param	7538/454	5736/379	5875/4874	6843/9556	5294/334	19136/721
θ range/deg	3.571−28.944	3.758−26.998	3.552−26.997	2.1796−30.5082	3.732−26.998	2.641−33.499
collected/unique reflns	21949/7538	17343/5736	16230/5875	88898/6843	26788/5294	108498/19136
R_1, wR_2 [$I > 2\sigma(I)$]	0.0668, 0.1775	0.0404, 0.0857	0.0816, 0.1746	0.0406, 0.0891	0.0292, 0.0636	0.0475, 0.0988
R_1, wR_2 (all data)	0.0979, 0.1897	0.0645, 0.0979	0.0966, 0.1825	0.0751, 0.1053	0.0369, 0.0678	0.0815, 0.1153
GOF(F^2)	0.956	1.038	1.191	1.052	1.033	1.030

Table 2. Selected Experimental Bond Lengths, Angles, and NO Frequencies for Crystals of the {RuNO}^{6,7} Species

	[**2-NO**]$(ClO_4)_3\cdot H_2O$	[**1-NO**]$(BF_4)_3$	[**3-NO**]$(BF_4)_3\cdot 2H_2O$	[**2-NO**]$(BF_4)_{1.97}I_{0.03}$[a]	[**1-NO**]$(BF_4)_2$	[**3-NO**]$(BF_4)_2$[b]
			Distances/Å			
Ru−N_1	1.762(4)	1.761(2)	1.776(5)	1.839(2)	1.852(2)	1.851(2)
Ru−N_2	2.125(4)	2.123(3)	2.110(6)	2.183(8)	2.169(2)	2.166(2)
Ru−N_3	2.165(4)	2.134(3)	2.138(6)	2.172(7)	2.151(2)	2.133(2)
Ru−N_4	2.156(4)	2.152(2)	2.132(6)	2.113(7)	2.145(2)	2.132(2)
Ru−N_5	2.113(4)	2.137(3)	2.138(5)	2.116(2)	2.113(2)	2.122(2)
Ru−N_6	2.122(4)	2.120(3)	2.153(5)	2.126(2)	2.109(2)	2.120(2)
N_1−O_1	1.119(6)	1.128(3)	1.133(7)	1.160(4)	1.177(3)	1.184(3)
			Angles/deg			
Ru−N_1−O_1	175.3(4)	173.2(3)	172.2(5)	144.2(2)	141.6(2)	141.2(2)
ν_{NO}/cm^{-1}	1925	1919	1947	1606	1611	1606

[a]The informed values correspond to the major component of the two disordered positions (Figure S5). [b]Average values for the nonequivalent molecules present in the unit cell (Figure S6).

Table 3. Selected Calculated (DFT; See the Text for Details) Bond Lengths, Angles, and NO Frequencies for the {RuNO}^{6,7} Species

	[**2-NO**]$^{3+}$	[**1-NO**]$^{3+}$	[**3-NO**]$^{3+}$	[**2-NO**]$^{2+}$	[**1-NO**]$^{2+}$	[**3-NO**]$^{2+}$
			Distances/Å			
Ru−N_1	1.78	1.78	1.79	1.90	1.90	1.90
Ru−N_2	2.19	2.18	2.18	2.22	2.22	2.22
Ru−N_3	2.24	2.23	2.22	2.23	2.23	2.22
Ru−N_4	2.23	2.22	2.20	2.22	2.22	2.21
Ru−N_5	2.13	2.16	2.19	2.15	2.15	2.16
Ru−N_6	2.15	2.18	2.19	2.16	2.16	2.17
N_1−O_1	1.18	1.18	1.18	1.22	1.22	1.22
			Angles/deg			
Ru−N_1−O_1	179.3	179.6	179.3	142.4	142.4	142.1
ν_{NO}/cm^{-1}	1848	1857	1860	1614	1620	1625

can be isolated by the addition of the appropriate counteranions (BF_4^-,PF_6^-, and ClO_4^-) or may be reacted in situ with nitrite to generate the corresponding [Ru(Me_3[9]aneN_3)(L^2)-(NO_2)]$^+$ nitro complexes. Acidification yields the {RuNO}^{6} nitrosyl complex [Ru(Me_3[9]aneN_3)(L^2)(NO)]$^{3+}$, which can be isolated as ClO_4^- or BF_4^- salt. Reaction of the latter species

DOI: 10.1021/acs.inorgchem.8b01958
Inorg. Chem. XXXX, XXX, XXX−XXX

with iodide in acetone allows for one-electron reduction, leading ultimately to the corresponding {RuNO}^{7} [Ru(Me$_3$[9]aneN$_3$)(L^2)(NO)]$^{2+}$ species (Figure 1).[18]

The appropriate selection of the crystallization conditions (see the Experimental Section) allowed us to obtain single crystals of the three {RuNO}^{6} compounds [Ru(Me$_3$[9]aneN$_3$)(bpy)(NO)]$^{3+}$ ([**1-NO**]$^{3+}$), [Ru(Me$_3$[9]aneN$_3$)(MeObpy)(NO)]$^{3+}$ ([**2-NO**]$^{3+}$), and [Ru(Me$_3$[9]aneN$_3$)(bpym)(NO)]$^{3+}$ ([**3-NO**]$^{3+}$) (Figure 2, left column) and the three {RuNO}^{7} ones [**1-NO**]$^{2+}$, [**2-NO**]$^{2+}$, and [**3-NO**]$^{2+}$ (Figure 2, right column).

Table 1 resumes the crystallographic information for the new species, and Tables 2 and 3 collect the most significant experimental and theoretical structural parameters, respectively. The {RuNO}^{6} complexes have very similar coordination environments and are almost superimposable if considering only the first-atom coordination sphere. The most relevant features in all of them are the short N$_1$−O$_1$bond lengths (average of 1.127 ± 0.005 Å) and the almost linear Ru−N$_1$−O$_1$ moieties (173.6 ± 0.4°), characteristic of the {MNO}^{6} species.[36] The vibrational frequencies associated with the stretching of the NO bond (ν_{NO}) are all close to 1900 cm^{-1} and are also typical of this kind of species (Table 2).[36] Overall, the identity of L^2 seems to have a negligible impact on the geometries. Nonetheless, DFT computations in vacuo predict slight structural changes: lengthening and shortening of the N$_1$−O$_1$ and Ru−N$_1$ bonds, respectively, in the sequence [**3-NO**]$^{3+}$, [**1-NO**]$^{3+}$, and [**2-NO**]$^{3+}$, following the increment in the basicity of L^2 that impacts the back-bonding to the coordinated nitrosyl (Table 3). These subtle changes are experimentally obscured most probably because of packing effects. One-electron reduction induces remarkable geometry modifications of the Ru−N$_1$−O$_1$ moiety for the three L^2 coligands. Most significantly, lengthening of the N$_1$−O$_1$ and Ru−N$_1$ bonds by ca. 0.05 and 0.08 Å, respectively, and bending of the Ru−N$_1$−O$_1$ fragment by ca. 30° (Figure 2 and Table 2) can also be observed in the DFT-computed geometries (Table 3). The rest of the coordination sphere remains roughly unchanged with the exception of the Ru−N$_2$ bonds, which experience a noticeable lengthening by ca. 0.05 Å. These findings are in line with previous observations of the rare octahedral complexes which have been structurally characterized in both {MNO}$^{6/7}$ states (Table S1), [(PaPy$_3$)Fe(NO)]$^{2+/+}$, [Fe(cyclam-ac)(NO)]$^{3,2,1+}$, and [Fe(NO)("pyS$_4$")]$^{+/0}$ [cyclam-ac = 1,4,8,11-tetraazacyclotetradecane-1-acetic acid(−); PaPy$_3$H = *N*,*N*-bis(2-pyridylmethyl)-amine-*N*-ethyl-2-pyridine-2-carboxamide; "pyS$_4$" = 2,6-bis(2-mercaptophenylthiomethyl)pyridine(2−)].[37]

EPR Spectra and Electronic Structures of the {RuNO}^{7} Species. [**1-NO**]$^{2+}$, [**2-NO**]$^{2+}$, and [**3-NO**]$^{2+}$ are EPR-active in frozen acetonitrile. Figure 3 displays the experimental X-band EPR spectra—and their fittings—for the three {RuNO}^{7} species, which resemble those reported for other {MNO}^{7} systems. The spectra display the typical $S = {}^1/_2$ signature of the {MNO}^{7} fragment,[4c,18,37a,e,38] with rhombic g values and hyperfine interaction with a single ^{14}N nucleus (I = 1). EPR spectra of {RuNO}^{7} systems have been described as roughly insensitive to the nature of the coligand environment,[38c] without any evident dependency with the nature of the coligands.

In the present case, however, the spin-Hamiltonian parameters (Table 4) correlate with the donor/acceptor properties of L^2.

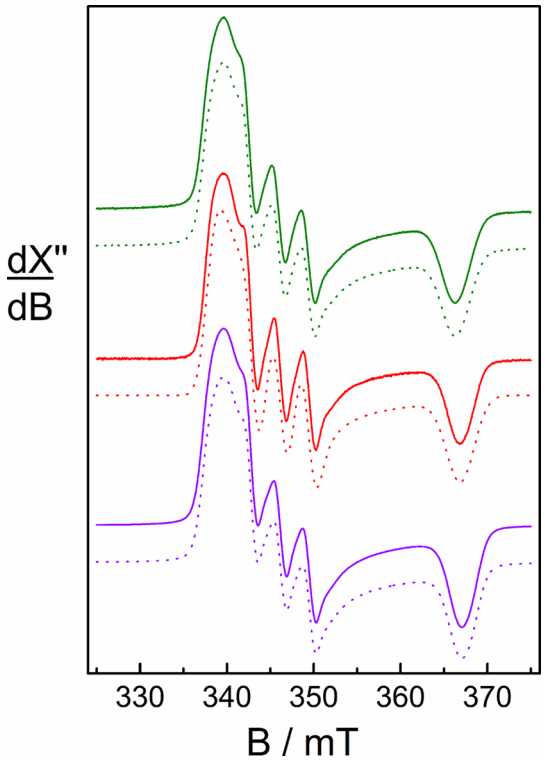

Figure 3. X-band EPR spectra of [**1-NO**]$^{2+}$ (red), [**2-NO**]$^{2+}$ (violet), and [**3-NO**]$^{2+}$ (green) in dry CH$_3$CN/Bu$_4$NPF$_6$ (0.2 M) at 85 K. Experimental spectra as full lines and computer-simulated spectra as dotted lines (details in the text). Microwave frequencies: 9.6487 GHz for [**1-NO**]$^{2+}$, 9.6478 GHz for [**2-NO**]$^{2+}$, and 9.6496 GHz for [**3-NO**]$^{2+}$.

The average g value and anisotropy of the principal values of the **g** matrix (Δg) increase slightly (beyond the uncertainty of the estimation) in the order [**3-NO**]$^{2+}$, [**1-NO**]$^{2+}$, and [**2-NO**]$^{2+}$, suggesting an increment of the spin density on the metal fragment as the donor capability of L^2 grows. Likewise, an exploration of the largest component of the ^{14}N hyperfine coupling tensor (A_2) indicates a decrease in the spin density on the N atom of NO along the same series. We conclude that these trends are due to higher spin delocalization from the NO ligand to the Ru center with increasing donor capabilities of the L^2 ligand. This apparently counterintuitive progression is reproduced by our DFT computations, as depicted by both the Mulliken spin densities and the orbital compositions of the singly occupied molecular orbitals (SOMOs) of the {RuNO}^{7} species (Table 5).

Figures 4 and S7 represent the computed SOMOs, which result from the predominantly σ overlap between the d$_{z^2}$ (and to a lower extent the d$_{xz}$) Ru orbitals and the NO-centered π^* orbital. The augmented spin delocalization from NO to Ru is the result of an increase in energy of the d$_{Ru}$ orbitals, when L^2 behaves as a better donor. This draws the d-manifold closer in energy to the π^* orbital (mainly centered in the NO ligand), thus enhancing not only the spin delocalization but most noticeably the σ-trans effect characteristic of {MNO}^{7} species and relevant in the bioinorganic field.[3a,4a,c,39] The σ-trans effect is, in fact, also behind the observed lengthening of the Ru−N$_2$ bond, and a careful comparison of this bond length along the series (Table 2) is actually consistent with the trends described above.

DOI: 10.1021/acs.inorgchem.8b01958
Inorg. Chem. XXXX, XXX, XXX−XXX

Table 4. EPR Spectroscopic Data of the {RuNO}^{7} Species[a]

	g_1	g_2	g_3	Δg	$g_{av.}$[b]	A_1	A_2	A_3
[**3-NO**]$^{2+}$	2.0312(1)	1.9926(1)	1.8823(1)	0.1488(2)	1.9697(1)	12.1(2)	30.42(9)	n.d.
[**1-NO**]$^{2+}$	2.0303(1)	1.9916(1)	1.8792(1)	0.1511(1)	1.9681(1)	10.96(7)	30.35(5)	n.d.
[**2-NO**]$^{2+}$	2.0307(1)	1.9911(1)	1.8780(1)	0.1527(2)	1.9676(1)	12.7(1)	29.8(1)	n.d.

[a]X-band EPR spectra obtained in CH_3CN/Bu_4NPF_6 (0.2 M) at 85 K. A_1, A_2, and A_3 are shown in units of 10^{-4} cm^{-1}. The numbers in parentheses show the 95% confidence interval. [b]$g_{av.}$ is calculated from $g_{av.} = [(g_1^2 + g_2^2 + g_3^2)/3]^{1/2}$.[38c] n.d.: not distinguishable from 0.

Table 5. Mulliken Spin Densities Calculated (DFT) for the {RuNO}^{7} Species

	Mulliken δ_{spin}		orbital composition of the SOMOs/%	
	Ru	NO	Ru	NO
[**3-NO**]$^{2+}$	0.0826	0.874	18.4	76.1
[**1-NO**]$^{2+}$	0.0876	0.871	19.5	75.2
[**2-NO**]$^{2+}$	0.0960	0.864	20.5	74.3

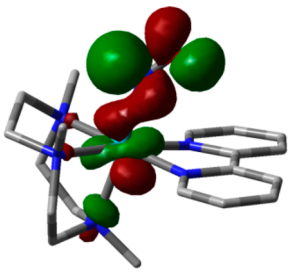

[**1-NO**]$^{2+}$

Figure 4. SOMO of the species [**1-NO**]$^{2+}$, computed after a corresponding orbital transformation.[40]

Redox Behavior. [**1-NO**]$^{2+}$, [**2-NO**]$^{2+}$, and [**3-NO**]$^{2+}$ are redox-active in an acetonitrile solution, and two reversible processes can be observed in their cyclic voltammograms (Figures 5 and Table S2). Controlled potential coulometry and UV−vis spectroelectrochemistry confirm the one-electron nature of both processes. The spectral changes associated with one-electron oxidation and one-electron reduction of {RuNO}^{7} (Figures S8−S10) are consistent with our previous report with L^2 = bpy as the coligand. The most important spectral features are well reproduced by TDDFT (Figures S15 and S16). The redox potentials for the {RuNO}$^{6/7}$ and {RuNO}$^{7/8}$ couples are strongly dependent on the identity of L^2, decreasing along the series [**3-NO**]$^{n+}$, [**1-NO**]$^{n+}$, and [**2-NO**]$^{n+}$. This sequence can also be ascribed to the donor properties of L^2 in the respective compounds, although it is worth noticing that the redox behavior seems to be more sensitive than the structural parameters.

Calculation of the redox potentials by means of DFT is not a straightforward procedure. An estimation can be obtained using an approach inspired by Van Stappen et al.[41] To minimize the complications associated with the theoretical evaluation of the solvation effects and the computation of the entropic contribution to the free energy variation along the redox process, the *difference* of the redox potentials between the half-reaction of interest and a well-defined half-reaction of reference involving a similar redox couple can be computed. In our case, this role is played by [**1-NO**]$^{n+}$, allowing one to estimate the redox potentials for the remaining {RuNO}$^{6/7}$ and {RuNO}$^{7/8}$ couples (more details can be found in the Supporting Information). The structural similarity between

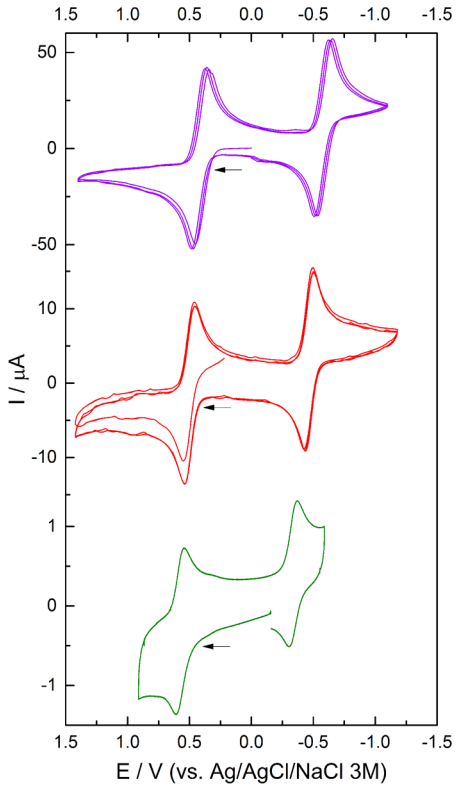

Figure 5. Comparison of the cyclic voltammograms obtained for [**1-NO**]$^{2+}$ (red), [**2-NO**]$^{2+}$ (violet), and [**3-NO**]$^{2+}$ (green) in dry CH_3CN/Bu_4NPF_6 (0.2 M) at 298 K. Scan rate = 100 mV·s^{-1}. *E* versus Ag/AgCl/NaCl (3 M).

the {RuNO} species of choice grants an appropriate compensation of errors along the procedure, yielding very good agreement with the experimental trends in spite of the simplicity of the approach (Table S3). Note that the agreement is better for the {RuNO}$^{7/8}$ couple than for the {RuNO}$^{6/7}$ case because of the lesser impact of the solvation effects for less charged species. The fairly good agreement observed in Table S3 validates the level of theory that we employed to gain insight into the electronic structure picture of our systems, also suggesting that this simple methodology can be used in a predictive way to estimate the redox properties of {MNO}$^{6/7/8}$ systems once a member of the family is properly characterized.

Bioinorganic Relevancy: Construction of Pourbaix Diagrams and Determination of the Acidity of Bound HNO. The solubility of the reported {RuNO}$^{6/7}$ species in water opens for the first time the door to study the influence on several properties caused by the systematic change of the coordination sphere. As was already reported for several {MNO}^{6} systems,[42] [**1-NO**]$^{3+}$, [**2-NO**]$^{3+}$, and [**3-NO**]$^{3+}$ undergo electrophilic attack by OH^- ions and convert into the corresponding nitro complexes according to eq 1.

DOI: 10.1021/acs.inorgchem.8b01958
Inorg. Chem. XXXX, XXX, XXX−XXX

$$[Ru(Me_3[9]aneN_3)(L^2)(NO)]^{3+} + 2OH^- \overset{K_{eq}}{\rightleftarrows} [Ru(Me_3[9]aneN_3)(L^2)(NO_2)]^+ + H_2O \quad (1)$$

Table S4 collects the equilibrium constants for the three complexes, which increase when L^2 becomes a weaker donor or, in other words, when the back-bonding to the nitrosyl fragment is less efficient. In an acidic solution, the redox couples $[\mathbf{1\text{-}NO}]^{3+/2+}$, $[\mathbf{2\text{-}NO}]^{3+/2+}$, and $[\mathbf{3\text{-}NO}]^{3+/2+}$ are observed to interconvert reversibly in CV and coulometry experiments despite the different time scales (Figures S11 and S12), with an electrochemical behavior that is fully independent of the original source employed to prepare the solutions (either the $\{RuNO\}^6$ or $\{RuNO\}^7$ isolated species). In alkaline solutions, the nitro species $[\mathbf{1\text{-}NO_2}]^+$, $[\mathbf{2\text{-}NO_2}]^+$, and $[\mathbf{3\text{-}NO_2}]^+$ are not electroactive, and no reduction of the sixth ligand is possible. On the contrary, basic solutions of $[\mathbf{1\text{-}NO}]^{2+}$, $[\mathbf{2\text{-}NO}]^{2+}$, and $[\mathbf{3\text{-}NO}]^{2+}$ can be oxidized irreversibly through an EC mechanism that involves first conversion into the corresponding $\{RuNO\}^6$ species and then attack of OH^- to finally yield the nitro derivatives.

In the solid state, the 2+ cations are easy to handle, even in the presence of air, but once they are dissolved in water, they react with O_2 to yield the corresponding 3+ species.[18] Nonetheless, all of them remain stable for hours under Ar, allowing for a systematic investigation under different pH conditions. Because the $[Ru(Me_3[9]aneN_3)(L^2)(NO)]^{2+}$ species are not affected by any acid−base-related phenomena, they stand as much more suitable starting materials than the corresponding $[Ru(Me_3[9]aneN_3)(L^2)(NO)]^{3+}$ to explore the pH dependence of the redox processes. Simple CV and SWV determinations performed on their solutions covering a broad pH range provide complete information to build the potential−pH Pourbaix diagrams, avoiding the somewhat cumbersome procedure we reported previously to explore the L^2 = bpy case, starting from the $\{RuNO\}^6$ analog. The $\{RuNO\}^7$ species undergo clean one-electron oxidation and one-electron reduction processes. CV or SWV determinations show that while the redox potentials for the different $\{RuNO\}^{6/7}$ couples remain practically constant independently of the acidity conditions, the $\{RuNO\}^{7/8}$ redox processes are strongly pH-dependent (Figure S13 for $[\mathbf{2\text{-}NO}]^{2+}$). As we already observed for L^2 = bpy,[16] two well-distinct regions can be identified: the high-pH region, where the redox potential remains independent of the pH, and the acidic region, where the redox potential decreases roughly 60 mV per pH unit. Spectroelectrochemistry (Figures 6, S11, S12, and S14−S16) and controlled potential coulometry confirm the one-electron nature of the redox events and reveal two distinct spectra for the species obtained upon reduction in alkaline or acidic conditions. The former situation corresponds to the actual $\{RuNO\}^{7/8}$ one-electron conversion represented in eq 2, while the latter involves a pH-dependent proton-coupled one-electron reduction (eq 3).

$$[Ru(Me_3[9]aneN_3)(L^2)(NO)]^{2+} + e^- \rightarrow [Ru(Me_3[9]aneN_3)(L^2)(NO)]^+ \quad (2)$$

$$[Ru(Me_3[9]aneN_3)(L^2)(NO)]^{2+} + e^- + H^+ \rightarrow [Ru(Me_3[9]aneN_3)(L^2)(HNO)]^{2+} \quad (3)$$

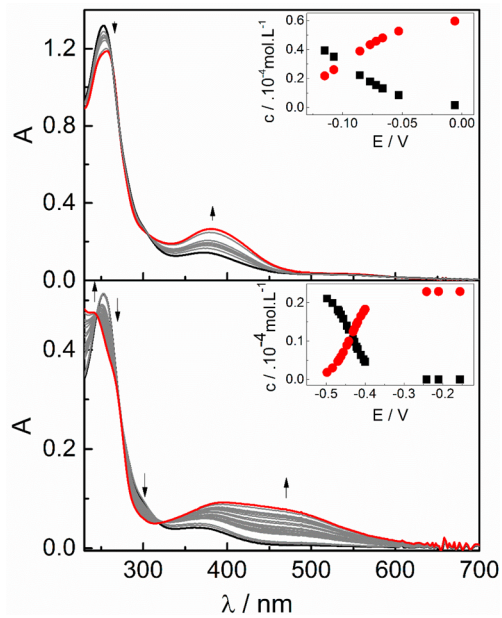

Figure 6. UV−vis spectra obtained by spectroelectrochemistry of $[\mathbf{3\text{-}NO}]^{2+}$ in aqueous media [I = 1 M NaCl and E vs Ag/AgCl/NaCl (3 M)] at 298 K under anaerobic conditions. The insets show the fraction of the different species as obtained from global analysis. Top: One-electron reduction at pH 2.5 (phosphate buffer). Bottom: One-electron reduction at pH 12.5 (phosphate buffer).

Figure 7 collects the redox information for $[\mathbf{2\text{-}NO}]^{n+}$. Individual plots for $[\mathbf{1\text{-}NO}]^{n+}$ and $[\mathbf{3\text{-}NO}]^{n+}$ can be found in Figures S17 and S18, respectively.

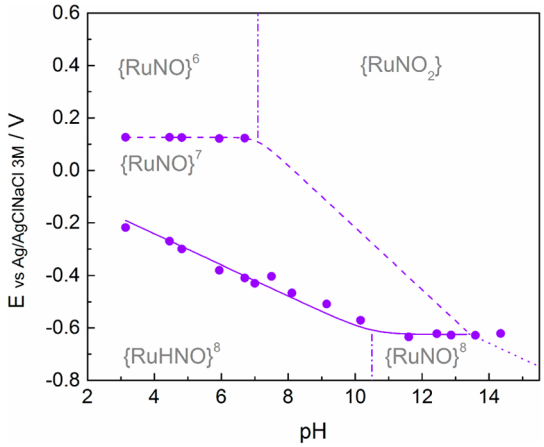

Figure 7. Pourbaix diagram of $[\mathbf{2\text{-}NO}]^{2+}$ obtained by CV/SWV/SEC in different buffer solutions [I = 1 M NaCl, at 298 K, E vs Ag/AgCl/NaCl (3 M)]. A nonlinear fitting of eq 6 to the experimental data yields $E^0_{NO/NO^-} = -0.625 \pm 0.008$ V and $pK_{a\ HNO} = 10.5 \pm 0.2$.

The solid line represents the best fit of eq 6 to the experimental data, which provides numerical values for the standard redox potentials associated with eqs 2 and 3 and K_a, the acidity constant of the coordinated HNO:

$$[Ru(Me_3[9]aneN_3)(L^2)(HNO)]^{2+} \overset{K_a}{\rightleftarrows} [Ru(Me_3[9]aneN_3)(L^2)(NO)]^+ + H^+ \quad (4)$$

DOI: 10.1021/acs.inorgchem.8b01958
Inorg. Chem. XXXX, XXX, XXX−XXX

$$E_{NO^+/NO_2^-\rightarrow NO^\bullet} = E^0_{NO^+/NO^\bullet} - \frac{RT}{F}\ln\left[1 + \frac{K_{eq}K_w^2}{(H^+)^2}\right] \quad (5)$$

$$E_{NO^\bullet\rightarrow NO^-} = E^0_{NO^\bullet/NO^-} - \frac{RT}{F}\ln\left[\frac{K_a}{K_a + (H^+)}\right] \quad (6)$$

$$E_{NO_2^-\rightarrow NO^-} = \frac{1}{2}(E^0_{NO^+/NO^\bullet} + E^0_{NO^\bullet/NO^-}) - \frac{RT}{2F}\ln\left[\frac{K_aK_{eq}K_w^2}{[K_a + (H^+)](H)^2}\right] \quad (7)$$

Figure 8 and Table 6 gather the comparative information collected for the three systems based on the different ligands L^2 described here. Some features of the diagrams show strong variation depending on L^2, while others show relative insensitivity to the chemical modifications of the complexes. The E^0 values for the redox couples $\{RuNO\}^{6/7}$ and $\{RuNO\}^{7/8}$ behave similarly, with a remarkable decrease in the order $[\mathbf{3\text{-}NO}]^{n+}$ > $[\mathbf{1\text{-}NO}]^{n+}$ > $[\mathbf{2\text{-}NO}]^{n+}$. The trends reflect the increasing donor properties of L^2, as we already described above (in an acetonitrile solution). The proton-coupled electron-reduction process resulting in the conversion of $\{RuNO\}^7$ into $\{RuHNO\}^8$ is roughly independent of the identity of L^2. This is a consequence of the simultaneous decrease in the reduction potential of the $\{RuNO\}^{7/8}$ couple and the enhancement of the protonation tendency of the resulting $\{RuNO\}^8$ species because of an increment in the donor properties of L^2. Both effects compensate, as shown in the thermodynamic cycle of Figure 9, and the derived potential versus pH curves remain insensitive to the chemical modification of the coligand, leaving the same standard redox potential (obtained by extrapolation to pH 0) at 0 V for the three couples.

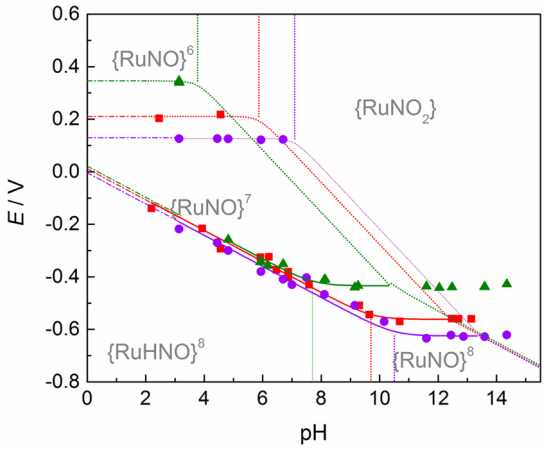

Figure 8. Comparison of the Pourbaix diagrams obtained for $[\mathbf{1\text{-}NO}]^{2+}$ (red), $[\mathbf{2\text{-}NO}]^{2+}$ (violet), and $[\mathbf{3\text{-}NO}]^{2+}$ (green) collected by CV/SWV/SEC in different buffer solutions [I = 1 M NaCl, at 298 K, E vs Ag/AgCl/NaCl (3 M)].

Table 6. Reduction Potentials and $pK_{a\ HNO}$ Obtained from the Pourbaix Diagrams

	$E^0_{NO/HNO}$/V	E^0_{NO/NO^-}/V	$pK_{a\ HNO}$
$[\mathbf{3\text{-}NO}]^{n+}$	0.021(5)	−0.434(4)	7.7(1)
$[\mathbf{1\text{-}NO}]^{n+}$	0.011(9)	−0.562(8)	9.7(2)
$[\mathbf{2\text{-}NO}]^{n+}$	−0.004(9)	−0.625(8)	10.5(2)

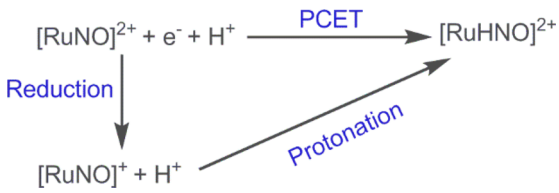

Figure 9. Thermodynamic cycle for the conversion of $\{RuNO\}^7$ into $\{RuHNO\}^8$, which shows insensitivity to the identity of L^2.

With respect to the general trends described above, the most striking result is the impressive change in the pK_a values of bound HNO spanning a range of three pH units triggered by relatively subtle modifications of L^2 with virtually no detectable structural changes of the complexes. The observed trend in pK_a of bound HNO is reproduced quite satisfactory by the DFT calculations for $[\mathbf{2\text{-}HNO}]^{2+}$ and $[\mathbf{3\text{-}HNO}]^{2+}$, related to $[\mathbf{1\text{-}HNO}]^{2+}$ (Table 7 and Figure S17), and reinforces that the main cause for the experimental trend arises from the donor/acceptor properties of the L^2 coligand.

Table 7. Comparison between the Experimental and Computed $pK_{a\ HNO}$ Values Referred to the One of $[\mathbf{1\text{-}HNO}]^{2+}$ [$\Delta(pK_{a\ HNO}) = pK_{a\ [x\text{-}HNO]^{2+}} - pK_{a\ [1\text{-}HNO]^{2+}}$]

	$pK^{EXP}_{a\ HNO}$	$\Delta(pK^{EXP}_{a\ HNO})$	$\Delta(pK^{DFT}_{a\ HNO})^a$
$[\mathbf{3\text{-}NO}]^{n+}$	7.7(1)	−2.0(3)	−3.3
$[\mathbf{1\text{-}NO}]^{n+}$	9.7(2)		
$[\mathbf{2\text{-}NO}]^{n+}$	10.5(2)	0.8(4)	1.6

[a]Calculations performed with geometries optimized in water (PCM). More details are given in the Supporting Information.

The linear correlation between pK_a values and the reduction potential for the $\{RuNO\}^{6/7}$ and the $\{RuNO\}^{7/8}$ conversions (Figure 10) is not completely unexpected, as both the pK_a and the reduction potentials are likewise affected by the electronic density modulation introduced by L^2.

■ CONCLUDING REMARKS

We highlighted the strong impact on the acidity of coordinated HNO induced by changes of the donor properties of coligands despite the fact that the structure stays essentially unchanged. Noticeably, the introduction of a weaker donor (or stronger π-acceptor) coligand can push the pK_a values to the physiological range. The possibility of deprotonation of coordinated HNO around pH 7 can certainly be of great bioinorganic relevance in order to elucidate the role of HNO/NO^- as a putative signaling system, given the strongly different binding abilities of each ligand, particularly reflected in the σ-trans effect and the reducing capabilities. Prior to our work, two biorelevant species containing bound HNO had been characterized in a water solution: the myoglobin adduct Mb-HNO[43] and the two-electron-reduced product of the nitroprusside anion ($[Fe(CN)_5NO]^{2-}$), namely $[Fe(CN)_5(HNO)]^{3-}$.[5,44] Whereas nitroprusside (containing formally bound NO^+) is not an endogenous species, it is currently used as a potential NO donor, where, supposedly, biological reductants favor the generation of the two-electron-reduced nitroxyl species. For the two above-mentioned examples, the pK_a values of bound HNO have been estimated as close to 10−11, although the case of $[Fe(CN)_5(HNO)]^{3-}$ needs a clarification.[41] In fact, the

DOI: 10.1021/acs.inorgchem.8b01958
Inorg. Chem. XXXX, XXX, XXX−XXX

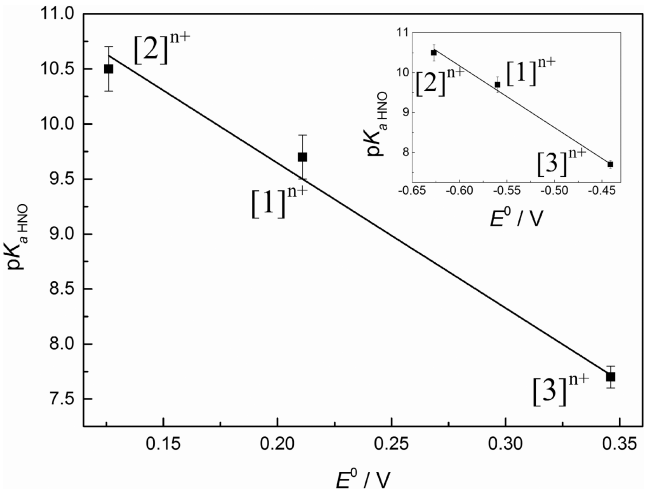

Figure 10. Correlation between pK_a of bound HNO and the reduction potential for the conversion of $\{RuNO\}^6$ into $\{RuNO\}^7$ [I = 1 M NaCl, at 298 K, E vs Ag/AgCl/NaCl (3 M)]. Linear fit parameters: p$K_{a\ HNO}$= −13; $E^0_{\{RuNO\}^6/\{RuNO\}^7}$ + 12.3; R^2 = 0.98596. Inset: Correlation between pK_a of bound HNO and the reduction potential for the conversion of $\{RuNO\}^7$ into $\{RuNO\}^8$ [measured under the same conditions, I = 1 M NaCl, at 298 K, E vs Ag/AgCl/NaCl (3 M)]. Linear fit parameters: p$K_{a\ HNO}$= −15; $E^0_{\{RuNO\}^7/\{RuNO\}^8}$ + 0.9; R^2 = 0.99245.

latter estimation, based on ^{17}O NMR measurements, appears as more reliable than the value of 7.7 obtained through a direct ^{1}H NMR titration experiment.[45] More relevant to our discussion, the interpretation of the nitroprusside results could be influenced by the change in the coordination number from hexacoordinated (6C) to pentacoordinated (5C), afforded through deprotonation and subsequent trans labilization of cyanide induced by NO^-. Accordingly, these kinds of effects could also influence macromolecules (like sGC) in which subtle structural changes in the protein environment can strongly impact its reactivity.[46] As a matter of fact, excess NO conditions promote an enhancement of sGC activity, together with the finding of a second-order rate law for the NO-concentration dependence. A detailed mechanistic picture of sGC activation is still lacking,[3b] although a plausible proposal of intermediate dinitrosyl formation and subsequent in situ nitroxyl (NO^-) generation could sustain a much more effective trans-activation effect than NO itself. Noticeably, the presently designed model system containing ruthenium chelate complexes avoids irreversible detachment of the N atom bound in the trans position, thus facilitating clean determination of the pK_a values of HNO with an essentially unchanged 6C environment, in contrast with trans labilizations, expected in complexes with monodentate ligands. Hence, rational modulation of the electronic properties introduced to the $\{RuNO\}^8$ fragment allows one to stabilize the complex bearing either an NO^- or an HNO ligand at physiological pH, contributing to clarification of the biological effect and (bio)relevancy that these small molecules may have. Indeed, the short lifetime of free HNO in aqueous media and its high binding ability to transition-metal centers point to a high relevance for better studying HNO-coordination chemistry, particularly with the heme model or adequately protein-substituted derivatives, given that not only sGC but also other prominent iron enzymes like NO synthases and NO reductases are mostly involved in the current biological functions of nitrosyl and nitroxyl species (NO^+, NO, and HNO/NO^-).[3b]

■ ASSOCIATED CONTENT

Supporting Information

The Supporting Information is available free of charge on the ACS Publications website at DOI: 10.1021/acs.inorgchem.8b01958.

Synthetic details for [**1-NO**]$(BF_4)_3$ and [**2-NO**]$(ClO_4)_3$, IR spectra, complementary computational details and results, crystallographic information on related compounds, structural representations of [**2-NO**]$(BF_4)_2$ and [**3-NO**]$(BF_4)_2$, redox potentials and spectroelectrochemical characterization in MeCN and H_2O, and complementary potential−pH diagrams (PDF)

Accession Codes

CCDC 1852505−1852507, 1852828, and 1852829 contain the supplementary crystallographic data for this paper. These data can be obtained free of charge via www.ccdc.cam.ac.uk/data_request/cif, or by emailing data_request@ccdc.cam.ac.uk, or by contacting The Cambridge Crystallographic Data Centre, 12 Union Road, Cambridge CB2 1EZ, UK; fax: +44 1223 336033.

■ AUTHOR INFORMATION

Corresponding Author

*E-mail: slep@qi.fcen.uba.ar.

ORCID

Pablo Alborés: 0000-0002-6181-4521
Thomas Weyhermüller: 0000-0002-0399-7999
Leonardo D. Slep: 0000-0001-6447-2216

Notes

The authors declare no competing financial interest.

■ ACKNOWLEDGMENTS

The authors thank the University of Buenos Aires, CONICET, the ANPCyT, and the DAAD for their financial assistance in conducting the research. We also mention the invaluable assistance of Dr. Eckhard Bill, who has made his laboratory available to us for the performance of EPR determinations. N.O.C., N.L., and J.P.M. received research grants from CONICET. P.A., J.A.O., and L.D.S. are members of the scientific staff of the same institution.

■ REFERENCES

(1) (a) Thomas, D. D.; Ridnour, L. A.; Isenberg, J. S.; Flores-Santana, W.; Switzer, C. H.; Donzelli, S.; Hussain, P.; Vecoli, C.; Paolocci, N.; Ambs, S.; Colton, C. A.; Harris, C. C.; Roberts, D. D.; Wink, D. A. The chemical biology of nitric oxide: Implications in cellular signaling. *Free Radical Biol. Med.* **2008**, *45*, 18−31. (b) Fukuto, J. M.; Carrington, S. J.; Tantillo, D. J.; Harrison, J. G.; Ignarro, L. J.; Freeman, B. A.; Chen, A.; Wink, D. A. Small Molecule Signaling Agents: The Integrated Chemistry and Biochemistry of Nitrogen Oxides, Oxides of Carbon, Dioxygen, Hydrogen Sulfide, and Their Derived Species. *Chem. Res. Toxicol.* **2012**, *25*, 769−793.

(2) Ignarro, J. L. E. *Nitric Oxide, Biology and Pathobiology*; Academic Press: San Diego, CA, 2000.

(3) (a) Traylor, T. G.; Sharma, V. S. Why nitric oxide? *Biochemistry* **1992**, *31*, 2847−2849. (b) Lehnert, N.; Berto, T. C.; Galinato, M. G. I.; Goodrich, L. E. The Role of Heme-Nitrosyls in the Biosynthesis, Transport, Sensing, and Detoxification of Nitric Oxide (NO) in Biological Systems: Enzymes and Model Complexes. *Handbook of*

DOI: 10.1021/acs.inorgchem.8b01958
Inorg. Chem. XXXX, XXX, XXX−XXX

Porphyrin Science; World Scientific Publishing Company, 2011; Vol. *14*, pp 1−247.

(4) (a) Goodrich, L. E.; Lehnert, N. The trans effect of nitroxyl (HNO) in ferrous heme systems: Implications for soluble guanylate cyclase activation by HNO. *J. Inorg. Biochem.* **2013**, *118*, 179−186. (b) Goodrich, L. E.; Roy, S.; Alp, E. E.; Zhao, J.; Hu, M. Y.; Lehnert, N. Electronic Structure and Biologically Relevant Reactivity of Low-Spin {FeNO}8 Porphyrin Model Complexes: New Insight from a Bis-Picket Fence Porphyrin. *Inorg. Chem.* **2013**, *52*, 7766−7780. (c) Levin, N.; Perdoménico, J.; Bill, E.; Weyhermuller, T.; Slep, L. D. Pushing the photodelivery of nitric oxide to the visible: are $\{FeNO\}^7$ complexes good candidates? *Dalton Trans* **2017**, *46*, 16058−16064.

(5) Bari, S. E.; Olabe, J. A.; Slep, L. D. Redox States of Metallonitrosyls in Aqueous Solution. *Adv. Inorg. Chem.* **2015**, *67*, 87−144.

(6) (a) Gratzel, M.; Taniguchi, S.; Henglein, A. Pulse radiolytic investigation of short-lived intermediates of the NO-reduction in aqueous solution. *Ber. Bunsen-Ges. Phys. Chem.* **1970**, *74*, 1003−1010. (b) Shafirovich, V.; Lymar, S. V. Nitroxyl and its anion in aqueous solutions: Spin states, protic equilibria, and reactivities toward oxygen and nitric oxide. *Proc. Natl. Acad. Sci. U. S. A.* **2002**, *99*, 7340. (c) Venancio, M. F.; Doctorovich, F.; Rocha, W. R. Solvation and Proton-Coupled Electron Transfer Reduction Potential of $^2NO^{\bullet}$ to ^1HNO in Aqueous Solution: A Theoretical Investigation. *J. Phys. Chem. B* **2017**, *121*, 6618−6625.

(7) (a) Fukuto, J. M.; Cisneros, C. J.; Kinkade, R. L. A comparison of the chemistry associated with the biological signaling and actions of nitroxyl (HNO) and nitric oxide (NO). *J. Inorg. Biochem.* **2013**, *118*, 201−208. (b) Fukuto, J. M. Recent History of HNO (Nitroxyl) Chemistry, Pharmacology and Therapeutic Potential. *Br. J. Pharmacol.* **2018**, DOI: 10.1111/bph.14384.

(8) Paolocci, N.; Jackson, M. I.; Lopez, B. E.; Miranda, K.; Tocchetti, C. G.; Wink, D. A.; Hobbs, A. J.; Fukuto, J. M. The pharmacology of nitroxyl (HNO) and its therapeutic potential: Not just the janus face of NO. *Pharmacol. Ther.* **2007**, *113*, 442−458.

(9) Doctorovich, F.; Farmer, P. J.; Martí, M. A. *The Chemistry and Biology of Nitroxyl (HNO)*, 1st ed.; Elsevier, 2016.

(10) Basudhar, D.; Bharadwaj, G.; Salmon, D. J.; Miranda, K. M. HNO Donors: Angeli's Salt and Related Diazeniumdiolates. In *The Chemistry and Biology of Nitroxyl (HNO)*, 1st ed.; Doctorovich, F., Farmer, P. J., Martí, M. A., Eds.; Elsevier, 2016; pp 11−36.

(11) Hamer, M.; Morales Vázquez, M. A.; Doctorovich, F. HNO: Redox Chemistry and Interactions with Small Inorganic Molecules. In *The Chemistry and Biology of Nitroxyl (HNO)*, 1st ed.; Doctorovich, F., Farmer, P. J., Martí, M. A., Eds.; Elsevier, 2016; pp 1−9.

(12) Bringas, M.; Semelak, J.; Zeida, A.; Estrin, D. A. Theoretical investigation of the mechanism of nitroxyl decomposition in aqueous solution. *J. Inorg. Biochem.* **2016**, *162*, 102−108.

(13) Fukuto, J. M.; Hobbs, A. J.; Ignarro, J. L. E. N,O-Diacylated-N-hydroxyarylsulfonamides: Nitroxyl precursors with potent smooth muscle relaxant properties. *Biochem. Biophys. Res. Commun.* **1993**, *196*, 707−713.

(14) (a) Doctorovich, F.; Bikiel, D. E.; Pellegrino, J.; Suárez, S. A.; Martí, M. A. Azanone (HNO) interaction with Hemeproteins and metalloporphyrins. *Adv. Inorg. Chem.* **2012**, *64*, 97−139. (b) Olabe, J. A.; Bari, S. E.; Slep, L. D. Non-Heme Transition Metal Complexes of HNO. In *The Chemistry and Biology of Nitroxyl (HNO)*, 1st ed.; Doctorovich, F., Farmer, P. J., Martí, M. A., Eds.; Elsevier, 2016; pp 127−153;. (c) Kumar, M. R.; Farmer, P. J. Spectroscopic NMR Characterizations of HNO Adducts of Ferrous Heme Proteins. In *The Chemistry and Biology of Nitroxyl (HNO)*, 1st ed.; Doctorovich, F., Farmer, P. J., Martí, M. A., Eds.; Elsevier, 2016; pp 269−285.

(15) (a) Roncaroli, F.; Videla, M.; Slep, L. D.; Olabe, J. A. New features in the redox coordination chemistry of metal nitrosyls {M-NO^+; M-$NO^{\bullet}$; M-NO^- (HNO)}. *Coord. Chem. Rev.* **2007**, *251*, 1903−1930. (b) Pellegrino, J.; Bari, S. E.; Bikiel, D. E.; Doctorovich, F. Successful Stabilization of the Elusive Species $\{FeNO\}^8$ in a Heme Model. *J. Am. Chem. Soc.* **2010**, *132*, 989−995.

(16) Codesido, N. O.; Weyhermüller, T.; Olabe, J. A.; Slep, L. D. Nitrosyl-Centered Redox and Acid−Base Interconversions in $[Ru(Me_3[9]aneN_3)(bpy)(NO)]^{3,2,1+}$. The pK_a of HNO for its Nitroxyl Derivative in Aqueous Solution. *Inorg. Chem.* **2014**, *53*, 981−997.

(17) (a) Enemark, J. H.; Feltham, R. D. Principles of Structure, Bonding, and Reactivity for Metal Nitrosyl Complexes. *Coord. Chem. Rev.* **1974**, *13*, 339−406. (b) Feltham, R. D.; Enemark, J. H. Structures of Metal Nitrosyls. *Top. Stereochem.* **2007**, *12*, 155−215.

(18) Levin, N.; Codesido, N. O.; Bill, E.; Weyhermuller, T.; Segantin Gaspari, A. P.; da Silva, R. S.; Olabe, J. A.; Slep, L. D. Structural, Spectroscopic, and Photochemical Investigation of an Octahedral NO-Releasing $\{RuNO\}^7$ Species. *Inorg. Chem.* **2016**, *55*, 7808−7810.

(19) Armarego, W. L. F.; Perrin, D. D. *Purification of Laboratory Chemicals*; Reed Educational & Professional Publishing Ltd., 1996.

(20) (a) Cheng, W. C.; Yu, W. Y.; Cheung, K. K.; Che, C. M. Syntheses of Novel Monomeric 1,4,7-Trimethyl-1,4,7- Triazacyclononane Ruthenium Complexes - Reactivities and Structure of Sterically Encumbered Cationic Monoaquaruthenium(Ii) and Monooxoruthenium(Iv) Complexes. *J. Chem. Soc., Dalton Trans.* **1994**, 57−62. (b) Vera, D. B.; Osa Codesido, N.; De Candia, A. G.; Alborés, P.; Slep, L. D. Chlorido(4,4'-dimethoxy-2,2'-bipyridine)-(1,4,7-trimethyl-1,4,7-triazacyclononane)ruthenium(II) perchlorate acetonitrile disolvate and aqua(4,4'-dimethoxy-2,2'-bipyridine)(1,4,7-trimethyl-1,4,7-triazacyclononane)ruthenium(II) bis(perchlorate) dihydrate. *Acta Crystallogr., Sect. C: Cryst. Struct. Commun.* **2012**, *68*, m127−130.

(21) Osa Codesido, N.; De Candia, A. G.; Weyhermuller, T.; Olabe, J. A.; Slep, L. D. An Electron-Rich $\{RuNO\}^6$ Complex: *trans*-$[Ru(DMAP)_4(NO)(OH)]^{2+}$ - Structure and Reactivity. *Eur. J. Inorg. Chem.* **2012**, *2012*, 4301−4309.

(22) Stoll, S.; Schweiger, A. EasySpin, a comprehensive software package for spectral simulation and analysis in EPR. *J. Magn. Reson.* **2006**, *178*, 42−55.

(23) (a) Gampp, H.; Maeder, M.; Meyer, C. J.; Zuberbühler, A. D. Quantification of a Known Component in an Unkown Mixture. *Anal. Chim. Acta* **1987**, *193*, 287−293. (b) Gampp, H.; Maeder, M.; Meyer, C. J.; Zuberbühler, A. D. Calculation of equilibrium constants from multiwavelength spectroscopic data — III Model-free analysis of spectrophotometric and ESR titrations. *Talanta* **1985**, *32*, 1133−1139. (c) Gampp, H.; Maeder, M.; Meyer, C. J.; Zuberbühler, A. D. Calculation of equilibrium constants from multiwavelength spectroscopic data — II SPECFIT: two user friendly programs in BASIC ans standard FORTRAN 77. *Talanta* **1985**, *32*, 257−264. (d) Gampp, H.; Maeder, M.; Meyer, C. J.; Zuberbühler, A. D. Calculation of equilibrium constants from multiwavelength spectroscopic data — I Mathematical considerations. *Talanta* **1985**, *32*, 95−101. (e) Malinovsky, E. R. *Factor Analysis in Chemistry*, 2nd ed.; Wiley-Interscience: New York, 1991.

(24) (a) Slep, L. D.; Mijovilovich, A.; Meyer-Klaucke, W.; Weyhermuller, T.; Bill, E.; Bothe, E.; Neese, F.; Wieghardt, K. Mixed-valent $\{Fe^{IV}(\mu\text{-}O)(\mu\text{-carboxylato})_2Fe^{III}\}^{3+}$ core. *J. Am. Chem. Soc.* **2003**, *125*, 15554−15570. (b) De Candia, A. G.; Marcolongo, J. P.; Slep, L. D. A new ruthenium nitrosyl species based on a pendant-arm 1,4,8,11-tetraazacyclotetradecane (cyclam) derivative: An experimental and theoretical study. *Polyhedron* **2007**, *26*, 4719−4730. (c) De Candia, A. G.; Singh, P.; Kaim, W.; Slep, L. D. All-*trans*-$[ClRu^{II}(py)_4(NC)Ru^{II}(py)_4(CN)Ru^{II}(py)_4(NO)](PF_6)_4$: A Redox-Active 2-Donor/1-Acceptor System Based on the Electrophilic $\{RuNO\}^6$ Motif. *Inorg. Chem.* **2009**, *48*, 565−573.

(25) (a) Roncaroli, F.; Baraldo, L. M.; Slep, L. D.; Olabe, J. A. Metallonitrosyl fragment as electron acceptor: Intramolecular charge transfer, long range electronic coupling, and electrophilic reactivity in the *trans*-$[NCRu(py)_4(CN)Ru(py)_4NO]^{3+}$ ion. *Inorg. Chem.* **2002**, *41*, 1930−1939. (b) Videla, M.; Jacinto, J. S.; Baggio, R.; Garland, M. T.; Singh, P.; Kaim, W.; Slep, L. D.; Olabe, J. A. New Ruthenium Nitrosyl Complexes with Tris(1-pyrazolyl)methane (tpm) and 2,2'-Bipyridine (bpy) Coligands. Structure, Spectroscopy, and Electrophilic and Nucleophilic Reactivities of Bound Nitrosyl. *Inorg. Chem.* **2006**, *45*, 8608−8617.

DOI: 10.1021/acs.inorgchem.8b01958
Inorg. Chem. XXXX, XXX, XXX−XXX

(26) *SCALE3 ABSPACK Empirical Absorption Correction, CrysAlis*; Oxford Diffraction Ltd., 2006.
(27) Altomare, A.; Burla, M. C.; Camalli, M.; Cascarano, G. L.; Giacovazzo, C.; Guagliardi, A.; Moliterni, A. G. G.; Polidori, G.; Spagna, R. SIR97: a new tool for crystal structure determination and refinement. *J. Appl. Crystallogr.* **1999**, *32*, 115−119.
(28) Sheldrick, G. M. A short history of SHELX. *Acta Crystallogr., Sect. A: Found. Crystallogr.* **2008**, *64*, 112−122.
(29) Farrugia, L. WinGX and ORTEP for Windows: an update. *J. Appl. Crystallogr.* **2012**, *45*, 849−854.
(30) *SADABS 2006/1*; Bruker AXS Inc.: Madison, WI, 2007.
(31) *ShelXTL 6.14*; Bruker AXS Inc.: Madison, WI, 2003.
(32) Sheldrick, G. M. *ShelXL97*; Universität Göttingen: Göttingen, Germany, 1997.
(33) Frisch, M. J. *Gaussian 09*, revision A.02; Gaussian Inc.: Wallingford, CT, 2009.
(34) (a) Becke, A. D. Density functional calculations of molecular bond energies. *J. Chem. Phys.* **1986**, *84*, 4524−4529. (b) Becke, A. D. Density-functional thermochemistry. III. The role of exact exchange. *J. Chem. Phys.* **1993**, *98*, 5648−5652. (c) Lee, C.; Yang, W.; Parr, R. G. Development of the Colle-Salvetti correlation-energy formula into a functional of the electron density. *Phys. Rev. B: Condens. Matter Mater. Phys.* **1988**, *37*, 785−789. (d) Perdew, J. P. Density-functional approximation for the correlation energy of the inhomogeneous electron gas. *Phys. Rev. B: Condens. Matter Mater. Phys.* **1986**, *33*, 8822−8824.
(35) (a) Dunning, T. H., Jr.; Hay, P. J. Modern Theoretical Chemistry. In *Modern Theoretical Chemistry*; Schaefer, H. F., III, Ed.; Plenum: New York, 1976; pp 1−28. (b) Hay, P. J.; Wadt, W. R. Ab initio effective core potentials for molecular calculations. Potentials for the transition metal atoms Sc to Hg. *J. Chem. Phys.* **1985**, *82*, 270−283. (c) Hay, P. J.; Wadt, W. R. Ab initio effective core potentials for molecular calculations. Potentials for K to Au including the outermost core orbitals. *J. Chem. Phys.* **1985**, *82*, 299−310. (d) Wadt, W. R.; Hay, P. J. Ab initio effective core potentials for molecular calculations. Potentials for main group elements Na to Bi. *J. Chem. Phys.* **1985**, *82*, 284−298.
(36) Olabe, J. A.; Slep, L. D. Reactivity and Structure of Complexes of Small Molecules: Nitric and Nitrous Oxide. In *Comprehensive Coordination Chemistry II, from Biology to Nanotechnology*; McCleverty, J. A., Meyer, T. J., Eds.; Elsevier: Oxford, U.K., 2004; Vol. *1*, pp 603−623.
(37) (a) Serres, R. G.; Grapperhaus, C. A.; Bothe, E.; Bill, E.; Weyhermuller, T.; Neese, F.; Wieghardt, K. Structural, spectroscopic, and computational study of an octahedral, non-heme $\{Fe\text{-}NO\}^{6-8}$ series: $[Fe(NO)(cyclam\text{-}ac)]^{2+/+/O}$. *J. Am. Chem. Soc.* **2004**, *126*, 5138−5153. (b) Sellmann, D.; Blum, N.; Heinemann, F. W.; Hess, B. A. Synthesis, reactivity, and structure of strictly homologous 18 and 19 valence electron iron nitrosyl complexes. *Chem. - Eur. J.* **2001**, *7*, 1874−1880. (c) Sellmann, D.; Gottschalk-Gaudig, T.; Haussinger, D.; Heinemann, F. W.; Hess, B. A. [Ru(HNO)('py(bu)S_4')], the first HNO complex resulting from hydride addition to a NO complex ('py(bu)S_4'$^{2-}$ = 2,6-bis(2- mercapto-3,5-di-*tert*-butylphenylthio)-dimethylpyridine(2-)). *Chem. - Eur. J.* **2001**, *7*, 2099−2103. (d) Patra, A. K.; Afshar, R.; Olmstead, M. M.; Mascharak, P. K. The First Non-Heme Iron(III) Complex with a Ligated Carboxamido Group That Exhibits Photolability of a Bound NO Ligand. *Angew. Chem., Int. Ed.* **2002**, *41*, 2512−2515. (e) Patra, A. K.; Rowland, J. M.; Marlin, D.; Bill, E.; Olmstead, M. M.; Mascharak, P. K. Iron nitrosyls of a pentadentate ligand containing a single carboxamide group: Syntheses, structures, electronic properties, and photolability of NO. *Inorg. Chem.* **2003**, *42*, 6812−6823.
(38) (a) McQuilken, A. C.; Ha, Y.; Sutherlin, K. D.; Siegler, M. A.; Hodgson, K. O.; Hedman, B.; Solomon, E. I.; Jameson, G. N. L.; Goldberg, D. P. Preparation of non-heme $\{FeNO\}^7$ models of cysteine dioxygenase: Sulfur versus nitrogen ligation and photorelease of nitric oxide. *J. Am. Chem. Soc.* **2013**, *135*, 14024−14027. (b) Wanner, M.; Scheiring, T.; Kaim, W.; Slep, L. D.; Baraldo, L. M.; Olabe, J. A.; Zalis, S.; Baerends, E. J. EPR characteristics of the $[(NC)_5M(NO)]^{3-}$ ions (M = Fe, Ru, Os). Experimental and DFT study establishing NO center dot as a ligand. *Inorg. Chem.* **2001**, *40*, 5704−5707. (c) Frantz, S.; Sarkar, B.; Sieger, M.; Kaim, W.; Roncaroli, F.; Olabe, J. A.; Zalis, S. EPR insensitivity of the metal-nitrosyl spin-bearing moiety in complexes $[L_nRu^{II}\text{-}NO^{\bullet}]^k$. *Eur. J. Inorg. Chem.* **2004**, *2004*, 2902−2907.
(39) Hunt, P.; Lehnert, N. Heme-Nitrosyls: Electronic Structure Implications for Function in Biology. *Acc. Chem. Res.* **2015**, *48*, 2117−2125.
(40) King, H. F.; Stanton, R. E.; Kim, H.; Wyatt, R. E.; Parr, R. G. Corresponding Orbitals and Nonorthogonality Problem in Molecular Quantum Mechanics. *J. Chem. Phys.* **1967**, *47*, 1936−1941.
(41) Van Stappen, C.; Goodrich, L. E.; Lehnert, N. The Interaction of HNO With Transition Metal Centers and Its Biological Significance. Insight Into Electronic Structure From Theoretical Calculations. In *The Chemistry and Biology of Nitroxyl (HNO)*, 1st ed.; Doctorovich, F., Farmer, P. J., Martí, M. A., Eds.; Elsevier, 2016; pp 155−192.
(42) Roncaroli, F.; Ruggiero, M. E.; Franco, D. W.; Estiu, G. L.; Olabe, J. A. Kinetic, mechanistic, and DFT study of the electrophilic reactions of nitrosyl complexes with hydroxide. *Inorg. Chem.* **2002**, *41*, 5760−5769.
(43) Sulc, F.; Immoos, C. E.; Pervitsky, D.; Farmer, P. J. Efficient Trapping of HNO by Deoxymyoglobin. *J. Am. Chem. Soc.* **2004**, *126*, 1096−1101.
(44) (a) Montenegro, A. C.; Amorebieta, V. T.; Slep, L. D.; Martin, D. F.; Roncaroli, F.; Murgida, D. H.; Bari, S. E.; Olabe, J. A. Three Redox States of Nitrosyl: NO^+, $NO^{\bullet}$, and NO^-/HNO Interconvert Reversibly on the Same Pentacyanoferrate(II) Platform. *Angew. Chem., Int. Ed.* **2009**, *48*, 4213−4216. (b) Montenegro, A. C.; Bari, S. E.; Olabe, J. A. Reactivity of iron(II)-bound nitrosyl hydride (HNO, nitroxyl) in aqueous solution. *J. Inorg. Biochem.* **2013**, *118*, 108−114.
(45) Gao, Y.; Toubaei, A.; Kong, X.; Wu, G. Acidity and Hydrogen Exchange Dynamics of Iron(II)-Bound Nitroxyl in Aqueous Solution. *Angew. Chem., Int. Ed.* **2014**, *53*, 11547−11551.
(46) Guo, Y.; Suess, D. L. M.; Herzik, M. A., Jr; Iavarone, A. T.; Britt, R. D.; Marletta, M. A. Regulation of nitric oxide signaling by formation of a distal receptor−ligand complex. *Nat. Chem. Biol.* **2017**, *13*, 1216.

DOI: 10.1021/acs.inorgchem.8b01958
Inorg. Chem. XXXX, XXX, XXX−XXX